

Title	Superconducting Transition of $RBa_{1-x}CuO_{3-x}$ (R : Y,Gd)
Author(s)	Mazaki, Hiromasa; Hiroi, Zenji; Takano, Mikio; Bando, Yoshichika; Kanno, Ryoji; Takeda, Yasuo; Yamamoto, Osamu
Citation	Bulletin of the Institute for Chemical Research, Kyoto University (1988), 65(5-6): 219-230
Issue Date	1988-03-15
URL	http://hdl.handle.net/2433/77206
Right	
Type	Departmental Bulletin Paper
Textversion	publisher

Superconducting Transition of $\text{RBa}_2\text{Cu}_3\text{O}_{7-x}$ (R: Y, Gd)

Hiromasa MAZAKI*, Zenji HIROI**, Mikio TAKANO**,
Yoshichika BANDO**, Ryoji KANNO***, Yasuo TAKEDA***,
and Osamu YAMAMOTO***

Received November 9, 1987

The superconducting transition of $\text{RBa}_2\text{Cu}_3\text{O}_{7-x}$ (R: Y, Gd) has been studied in terms of complex susceptibility and ac resistance. The structural examination of the samples was made by X-ray diffraction and transmission electron microscopy. The susceptibility measurements have revealed that the transition of a disk sample has two phases. One is insensitive to the change in the amplitude h_0 of the external ac magnetic field. The other is very sensitive to h_0 , where the transition width is appreciably broadened as h_0 increases. No frequency dependence is found below 320 Hz. The results suggest the superconducting transition of a disk sample takes place through the concurrence of the bulk and coupled phases. The ac-resistive measurement of a disk sample as well as the complex-susceptibility measurement of a powdered sample support the above results. Discussion was made in the framework of the phenomenological weak-link loop model.

KEY WORDS: Oxide superconductor/ Complex susceptibility/ Transition temperature/ Hartshorn bridge/

I. INTRODUCTION

Recently, a considerable effort has been made to understand the fundamental behaviors of oxide superconductors. We have attempted to investigate the superconductivity by means of complex susceptibility, $\chi = \chi' - i\chi''$. As is well known, the change in χ' with respect to temperature is caused by the Meissner effect. Meanwhile, χ'' is proportional to the energy dissipation in a specimen located in a periodically varying magnetic field. In order to confirm the zero-resistive state, the measurement of resistive transition is also essential.

Present investigation was made for two kinds of oxide superconductors, $\text{YBa}_2\text{Cu}_3\text{O}_{7-x}$ and $\text{GdBa}_2\text{Cu}_3\text{O}_{7-x}$. In this paper, we report the detailed study of the structure and the complex susceptibility of these systems. The ac resistive transition is also presented and comparison with the results of complex susceptibility was made. The observed results are discussed with an aid of the phenomenological weak-link loop model.

II. EXPERIMENTAL

1. Sample preparation

Samples of $\text{RBa}_2\text{Cu}_3\text{O}_{7-x}$ (R: Y, Gd, $x \approx 0.1$) were prepared from R_2O_3 , BaCO_3 , and CuO ,

* 間崎啓匡: Laboratory of Nuclear Radiation, Institute for Chemical Research, Kyoto University, Kyoto 606.

** 広井善二, 高野幹夫, 坂東尚周: Laboratory of Solid State Chemistry, Institute for Chemical Research, Kyoto University, Uji 611.

*** 菅野了次, 武田保雄, 山本 治: Department of Chemistry, Faculty of Engineering, Mie University, Tsu 514.

each with a purity above 99.9%. These raw materials were mixed thoroughly in an agate mortar, and pressed into pellets. Then they were heated at 1173 K (R=Y) and 1193 K (R=Gd) for 48 h with intermittent grinding, mixing, and pelletization. The atmosphere was air for R=Y and oxygen of 1 atm for R=Gd. The products were gradually cooled to 673 K and annealed at the same temperature for 48 h. The samples obtained were examined by X-ray diffraction (XRD) and transmission electron microscopy (TEM). The XRD patterns were monophasic for both R=Y and Gd. The lattice constants of the samples thus prepared are $a=0.3818$ nm, $b=0.3895$ nm, and $c=1.1665$ nm for $\text{YBa}_2\text{Cu}_3\text{O}_{6.86}$ and $a=0.3835$ nm, $b=0.3895$ nm, and $c=1.1780$ nm for $\text{GdBa}_2\text{Cu}_3\text{O}_{7-x}$ ($x \approx 0.1$). The oxygen deficiency of the sample with R=Y was determined as $x=0.14$ by thermogravimetry as described elsewhere.¹⁾ A similar value can be expected for the R=Gd sample.

The oxygen deficient tri-perovskite structure of $\text{YBa}_2\text{Cu}_3\text{O}_{6.86}$ was confirmed by observing both ED patterns and high resolution images in the TEM. In addition, microstructures which can not be identified by the XRD method are discussed. The advantage of the TEM observation is that the structural information of micro-regions can be obtained directly in the

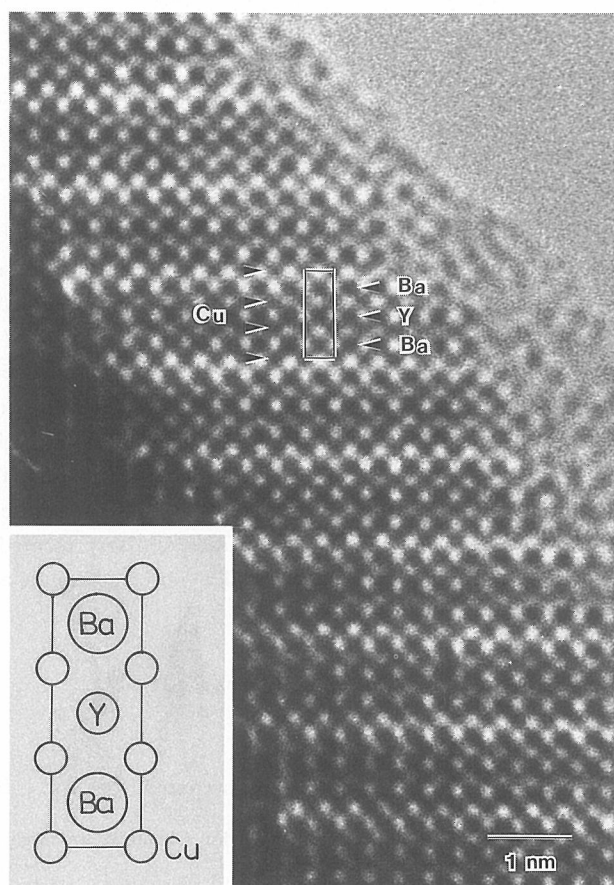


Fig. 1. High resolution structure image of $\text{YBa}_2\text{Cu}_3\text{O}_{6.86}$ taken with an incident electron beam along the [100] or [010] direction. A projection of the tri-perovskite structure is shown in the Inset.

real space by carefully interpreting the images. Samples for TEM were prepared by crushing as-prepared sintered pellets and dispersing with alcohol on a micro-grid. TEM observations were carried out by a 200-kV electron microscope (JEM-2000EX) equipped with a top entry goniometer.

Figure 1 demonstrates a high resolution structure image of $\text{YBa}_2\text{Cu}_3\text{O}_{6.86}$ taken with an incident electron beam along the $[100]$ or $[010]$ direction. An well ordered arrangement of white and black dots are clearly visualized in a stripped region near the sample edge where the sample thickness is thin enough. It is known that, under a proper imaging condition, a many-beam image of such a thin crystal can be interpreted as a two-dimensional projection of the charge density. So, the black dots may be assigned to arrays of heavy atoms and white ones to arrays of 'holes' surrounded by them, namely potential valleys. In the image, a

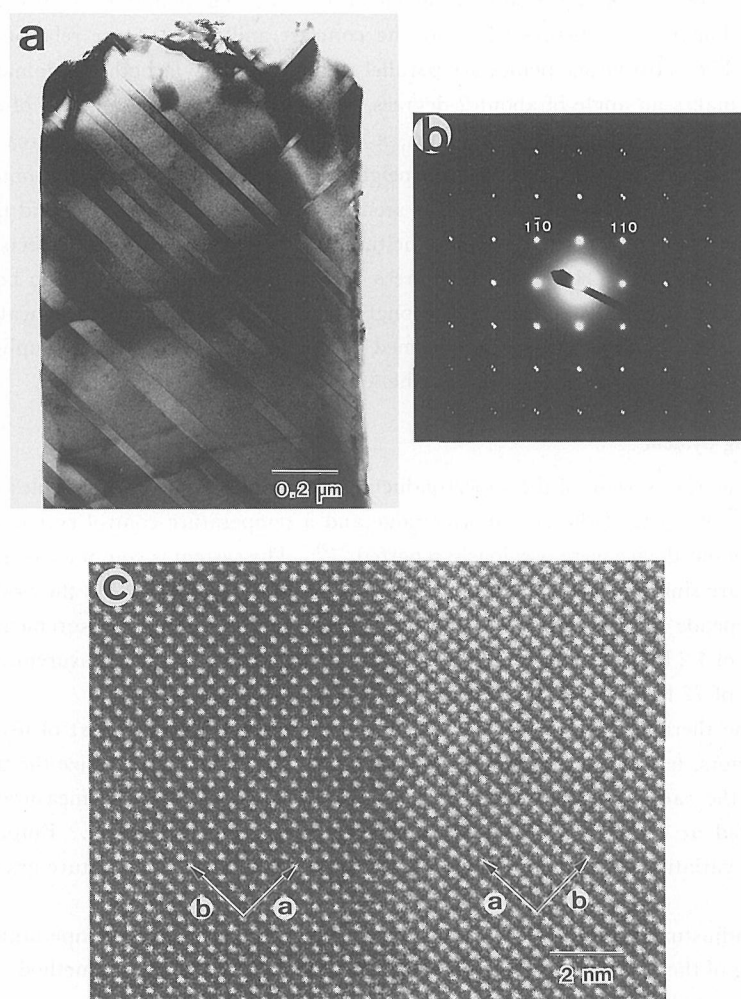


Fig. 2. (a) TEM micrograph of $\text{YBa}_2\text{Cu}_3\text{O}_{6.86}$ with a beam along the $[001]$ showing microtwin bands. (b) $[001]$ zone axis ED pattern corresponding to (a) showing splits due to the microtwinning. (c) High resolution image around a twin boundary. It can be formed by mirroring across the $(1\bar{1}0)$ plane.

two-dimensional unit cell with dimensions of a or $b=0.38$ nm and $c=1.17$ nm marked by a rectangle drawn can be clearly identified. The positions of the metal atoms along the c -axis are also shown considering that Ba and Y atoms correspond to larger black dots and Cu atoms to smaller ones. Thus, the structure image of the sample can be successfully explained by the tri-perovskite structure illustrated in the Inset of Fig. 1, in which Ba and Y at the A-sites of the perovskite have an ordered arrangement along the c -axis leading to the tripled c -axis.

Some characteristic stripped contrasts can be seen in images viewed along the c -axis. Figure 2(a) shows a typical image at a low magnification. Stripped variation of the contrast on a scale of from several tens to several hundreds of nanometers and some microcracks are clearly seen in the image. This striation has been regarded as twin lamellas introduced in the process of the structural change from the high-temperature tetragonal phase to the low-temperature orthorhombic one.^{2,3)} A high resolution image around the twin boundary is illustrated in Fig. 2(c). Two domains are distinguished by the contrast and have mirror relation across the boundary. The $(1\bar{1}0)$ lattice planes are parallel to the boundary in both the domains, but the (110) plane makes an angle of about 2 degrees, because the lattice parameters of a and b are slightly different ($b-a=6\times 10^{-2}\text{\AA}$). Thus, a diffraction pattern from this area consists of overlapping two sets of spots arising from neighboring domains. It should be noted that the $(h\bar{h}o)$ spots are common in the both sets as seen in Fig. 2(b). It has been found that most of the twin boundaries are very sharp and neither strain fields nor crystal defects like shear structures are observed. However, there are a few papers reporting faded twin boundaries.⁴⁾ The features of the twin boundaries may strongly depend on the method of the heat treatment. The coherent twin boundaries generally formed do not seem to lead to weak coupling between superconductive grains to be described in the following sections.

2. Measuring System

The measuring system of the superconducting transition by means of complex susceptibility, $\chi' - i\chi''$, consists of the Hartshorn bridge and a temperature control system (1–325 K). The details of our device were previously reported.^{5–7)} The system is computer-controlled, and χ' and χ'' are simultaneously measured as a function of temperature. As the bridge-balance condition depends on the coil temperature, we made the 4.2–100 K measurements at a coil temperature of 4.2 K (immersed in a liquid He bath) and the 80–100 K measurements at a coil temperature of 77 K (immersed in a liquid N₂ bath).

Since the thermal conductivity of the sample is poor compared to that of usual metallic superconductors, temperature was carefully controlled. In order to minimize the temperature gradient in the sample (or between the sample and thermometer), the measurement of χ always started at 130 K and the temperature was lowered quite slowly. Empirically, the temperature variation of 0.2 K/min does not cause an appreciable temperature gradient in the sample.

A null adjustment of the Hartshorn bridge was made at the sample temperature of 105 K. Phase setting of the lock-in analyzer was made by the so-called off-balance method. Temperature was measured with a calibrated carbon-glass thermometer.

For the measurement of a disk sample, the ac magnetic field, $h(t)=h_0\sin 2\pi ft$, was applied perpendicular to the flat surface of the disk. The demagnetizing effect was previously found not to be crucial for our experiment.⁸⁾ For the measurement of a powdered sample, it was

mounted in the sample room with Apieson N grease.

The complex susceptibility was measured at various amplitudes h_0 (5–1000 mOe), where the frequency f was fixed at 132 Hz. With different frequencies up to 320 Hz (h_0 is fixed), no appreciable change was found in the observed χ .

The measurement of ac-resistive transition was carried out by the conventional four-probe method. The ac current supplied to the disk sample was 1.9 mA, $f=132$ Hz.

III. RESULTS AND DISCUSSION

1. $\text{YBa}_2\text{Cu}_3\text{O}_{6.86}$

In Fig. 3, we show typical curves of χ' and χ'' ($h_0=5$ mOe, $f=132$ Hz), together with the curve of ac-resistive transition. The normal-state resistivity was estimated to be 0.75 m Ω cm at 100 K. Figures 4 and 5 present χ' and χ'' versus T for several different h_0 . From these figures, we note the following aspects.

(a) The transition of χ' is quite smooth, but seems to have two phases (the higher- and lower-temperature phases). The onset temperature of the higher-temperature phase, T_1 ($=93.6$ K), coincides with the onset of ac-resistive transition. At the onset temperature of

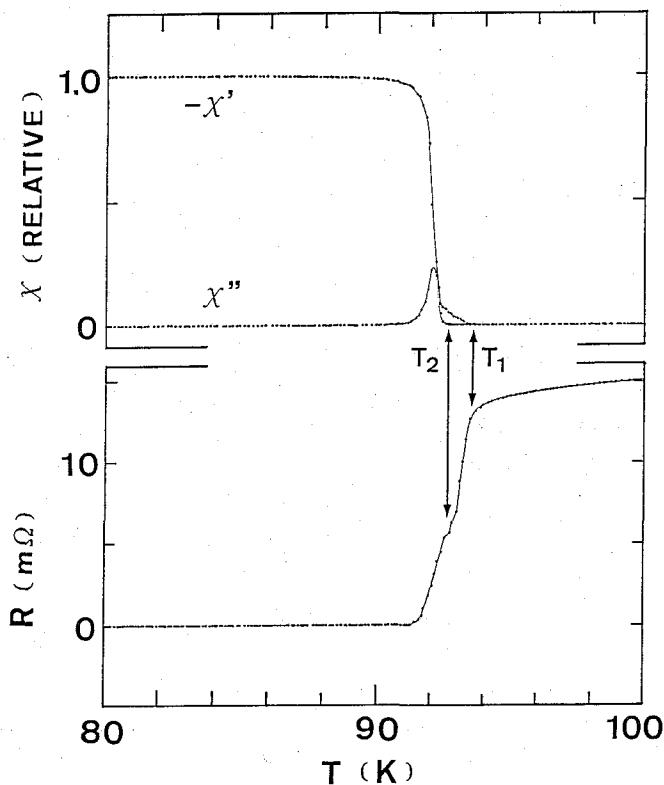


Fig. 3. Real and imaginary components of the susceptibility ($h_0=5$ mOe, $f=132$ Hz) and the ac-resistive transition curve (ac current=1.9 mA, $f=132$ Hz) of $\text{YBa}_2\text{Cu}_3\text{O}_{6.86}$ as a function of temperature. T_1 ($=93.6$ K) and T_2 ($=92.6$ K) denote the onset temperatures of χ' and χ'' , respectively. The transition width of χ' (10–90%) is 0.8 K.

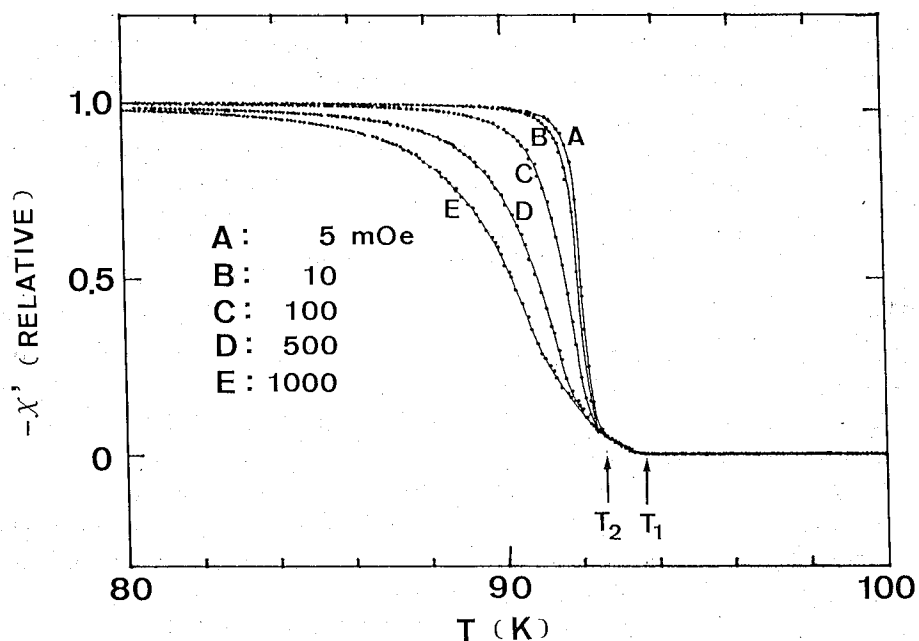


Fig. 4. Real component of the susceptibility of $\text{YBa}_2\text{Cu}_3\text{O}_{6.86}$ vs temperature for several different h_0 , where $f=132$ Hz.

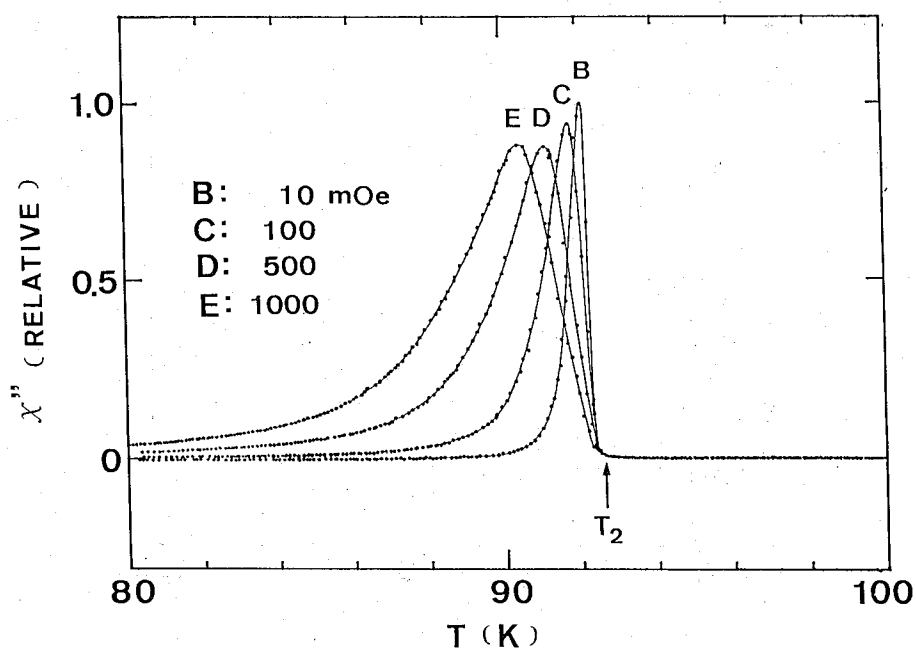


Fig. 5. Imaginary component of the susceptibility of $\text{YBa}_2\text{Cu}_3\text{O}_{6.86}$ vs temperature for several different h_0 , where $f=132$ Hz. Data for $h_0=5$ mOe is omitted for clarity.

the lower-temperature phase, $T_2(=92.6 \text{ K})$, the ac-resistive transition shows a slight instability and the slope alters.

(b) In the temperature region $T_2 < T < T_1$, χ'' does not appear (or may be quite small). When the temperature is lowered further, χ'' begins to form a single peak. The peak height has a maximum for $h_0 = 10 \text{ mOe}$.

(c) In the temperature region $T_2 < T < T_1$, χ'' does not depend on h_0 , where both T_1 and T_2 seem to be constant.

(d) For $T < T_2$, both χ' and χ'' depend sensitively on h_0 . Their transition widths broaden as h_0 increases.

Based on these experimental evidences, we attempt to reveal the superconducting characteristics of our sample. The insensitive nature of χ' to h_0 and the nearly zero value of χ'' in the temperature region $T_2 < T < T_1$ are undoubtedly the characteristics of a pure bulk superconductor. This fact suggests that at T_1 , fairly solid superconducting inclusions appear, and these inclusions spread over the sample volume as the temperature decreases.

When the temperature reaches T_2 , χ'' starts to form a peak. As seen in Figs. 4 and 5, both χ' and χ'' become very sensitive to h_0 below T_2 . This broadening of the transition curves is quite similar to that of a multiconnected network consisting of the weak-link Josephson junctions. This indicates that below T_2 , the superconducting inclusions begin to couple with each other and form a multiconnected network. It should be noted that the peak height of χ'' of the present sample has the maximum for $h_0 = 10 \text{ mOe}$. However, for another $\text{YBa}_2\text{Cu}_3\text{O}_{7-x}$ specimen, the height increases monotonically with the increase of h_0 . At the present stage, we cannot give a concrete explanation for the origin of this difference. This may come from the delicate balance between the production of superconducting inclusions and their coupling strength.

The above-mentioned coupling process is also reflected on the ac-resistive transition. As shown in Fig. 3 the ac-resistive curve shows a slight instability near T_2 and changes its slope. A similar behavior of the resistive transition curve has also been reported by others.⁹⁾ In addition, their results show that the latter half of the transition curve to the superconducting state depends on the external magnetic field.

Our previous research with metallic technetium embedded in a porous alumina revealed that the complex susceptibility of the multiconnected structure can be reproduced well by the phenomenological weak-link loop model.⁶⁾ In this model, the multiconnected network behaves like a single loop due to the coherent nature of the specimen. The curves of χ' and χ'' calculated by this model seem to reproduce the present results well in the temperature region of $T < T_2$ (see Fig. 6 of Ref. 6).

The frequency dependence of χ' and χ'' was also measured. Three different frequencies ($f = 50, 132, 320 \text{ Hz}$) were used, where h_0 was fixed at 100 mOe . We found that neither χ' nor χ'' was affected by the change in f . This fact strongly supports the proposal that the present system belongs more or less to the category of the weak-link loop model, and is not an average conductivity model.¹⁰⁾

Further confirmation of the above discussion was made by measuring χ of a powdered sample. A sample prepared by a similar treatment was divided into two pieces with one of them carefully powdered. Then, in order to ascertain the thermal contact, the powder was mounted in the sample room with Apieson N grease.

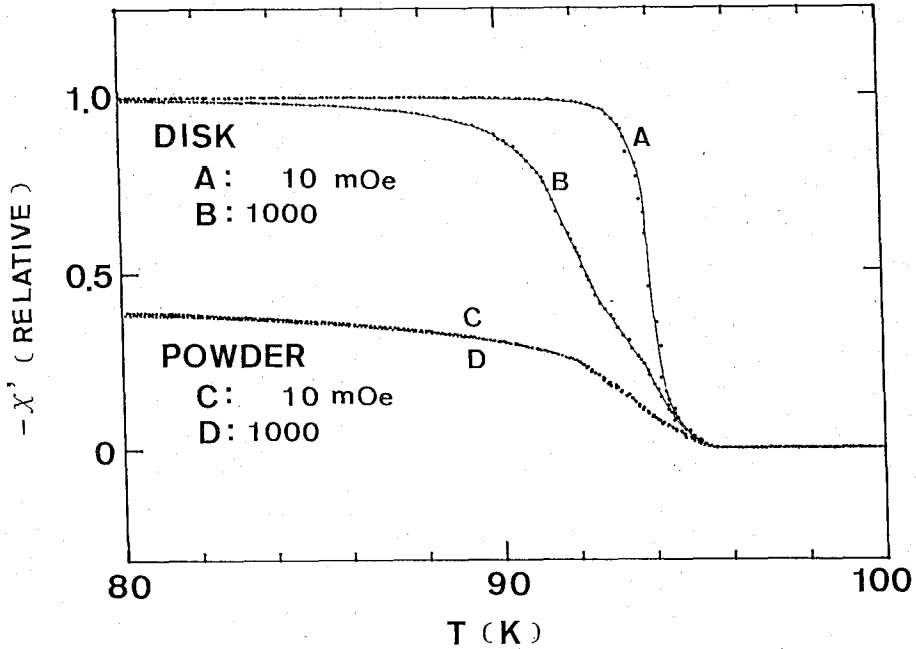


Fig. 6. Real component of the susceptibility for the disk and powdered $\text{YBa}_2\text{Cu}_3\text{O}_{6.86}$ vs temperature for two different h_0 . No h_0 dependence appears in the curve of the powdered sample.

As shown in Fig. 6, the h_0 dependence of the disk sample is essentially the same as those given in Figs. 4 and 5, although the onset temperature is higher by about 2 K. On the contrary, the observed χ of the powdered sample contrasted with that of the disk sample. As seen in the figure, χ' of the powdered sample was practically insensitive to h_0 in the whole temperature region measured. Furthermore, the peak in the χ'' transition curve completely disappears (not shown in the figure). From these, we believe that the weak-link junctions involved in the disk sample were almost completely destroyed by powdering.

2. $\text{GdBa}_2\text{Cu}_3\text{O}_{7-x}$

In Fig. 7, we show $-\chi', R$ versus T . As shown in Fig. 7 (a), the onset temperature T_1 of $-\chi'$ is the same for all h_0 measured. No h_0 dependence appears until the temperature is lowered to T_2 . Below T_2 , $-\chi'$ grows rather rapidly and shows an appreciable h_0 dependence. As illustrated in Fig. 7(b), the curve of ac-resistive transition apparently alters its slope at T_2 .

In Fig. 8, we give χ'' versus T . The onset temperature of χ'' is equal to T_2 , and does not depend on h_0 . χ'' forms a single peak which broadens as h_0 increases. It is noted that there are no visible changes in χ'' in the temperature region between T_1 and T_2 , where χ' converges on the single line. The peak height becomes smaller as h_0 increases, but almost saturates for $h_0 > 500$ mOe (not shown in the figure). No frequency dependence was observed in χ up to 320 Hz. These behaviors are quite similar to the Y-Ba-Cu-O system, and consequently the weak-link loop model is also applicable to the Gd-Ba-Cu-O system.

For further confirmation of the above consideration the disk sample used was carefully powdered, and then the powder was mounted in the sample room with Apieson N grease. As

Superconducting Transition of $\text{R}\text{Ba}_2\text{Cu}_3\text{O}_{7-x}$

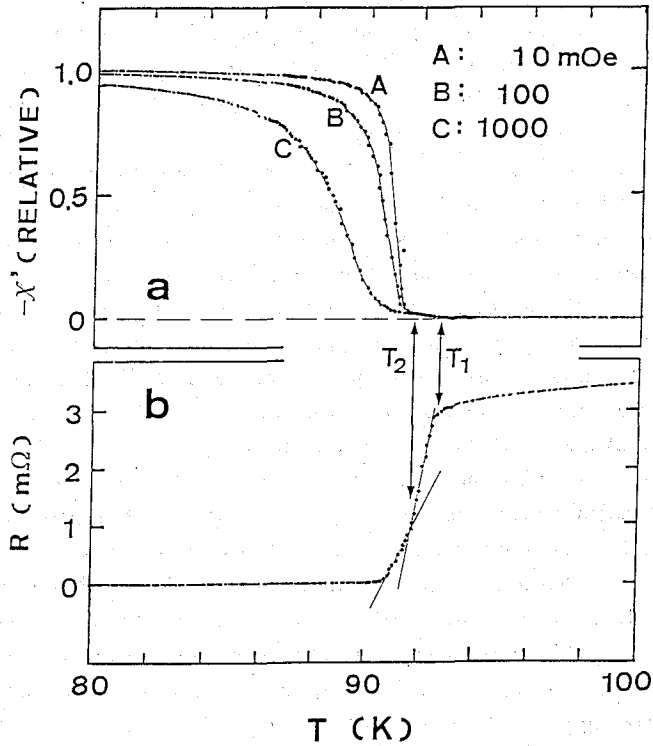


Fig. 7. Real components of the susceptibility for three different h_0 (a) and ac resistance (b) of $\text{Gd}\text{Ba}_2\text{Cu}_3\text{O}_{7-x}$ vs temperature. The ac current in (b) is 1.9 mA, and $f=132$ Hz for both (a) and (b). T_1 is the onset temperature of $-\chi'$. At T_2 , the coupling phase appears.

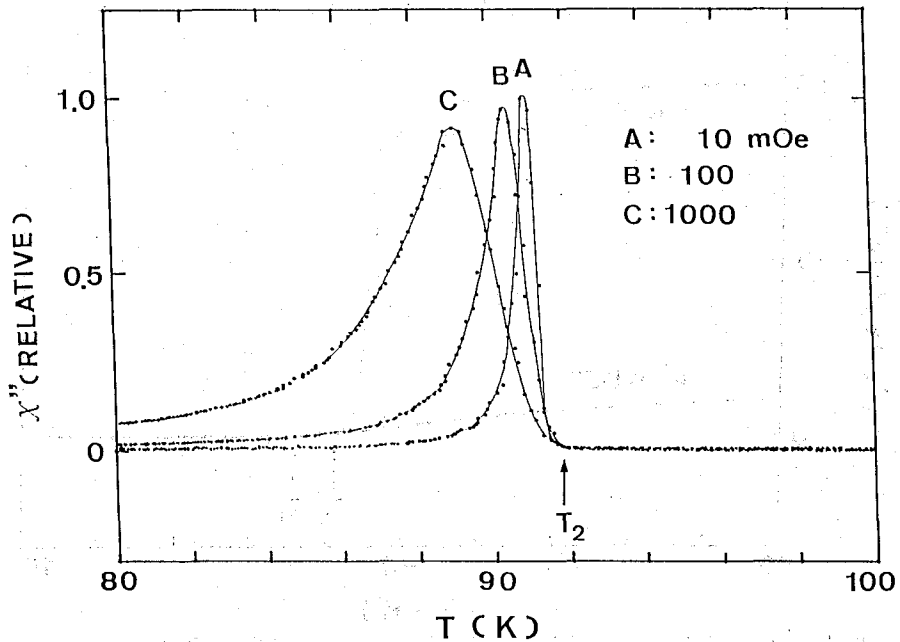


Fig. 8. Imaginary component of the susceptibility of $\text{Gd}\text{Ba}_2\text{Cu}_3\text{O}_{7-x}$ for three different h_0 vs temperature, where $f=132$ Hz. T_2 is the onset temperature of χ'' .

shown in Fig. 9, the growth of $-\chi'$ is greatly suppressed (11% of the sample at 80 K) and no rapid growth occurs at T_2 . In addition, χ'' does not appear in the whole temperature region (not shown in the figure). This indicates that the weak-coupling nature between the inclusions is almost completely destroyed. For quantitative discussion on this small value of $-\chi'$ in the powdered sample, we need to know the volume fraction of $\text{GdBa}_2\text{Cu}_3\text{O}_{7-x}$ in the disk sample as well as the field penetration length into the superconducting inclusions.

As the temperature is lowered further from 80 K, $-\chi'$ increases monotonically down to about 10 K. However, near this temperature, $-\chi'$ takes the maximum value and then decreases slightly with the decrease of temperature (see Fig. 10).

According to the work by Thompson et al.,¹¹⁾ superconductivity and field-induced paramagnetism in $\text{GdBa}_2\text{Cu}_3\text{O}_{7-x}$ exist independent of one another. Furthermore, it is suggested that the antiferromagnetic transition of Gd^{3+} occurs near 2 K.

From these results, we believe that the turning point in the curve of $-\chi'$ at about 10 K is due to the field-induced paramagnetism which is expected to be enhanced at very low temperatures. A slight increase of the complex susceptibility has been reported for the Tetra-II $\text{ErBa}_2\text{Cu}_3\text{O}_x$ (not superconductor), where χ begins to grow at about 20 K.¹²⁾

It should be noted that in our case, this turning point at about 10 K was not observed for the disk sample. It was visible only for the powdered sample. The reason for this is that in the disk sample, the field-induced paramagnetism in the superconducting inclusions hardly takes place due to the diamagnetic shielding current covering the whole specimen. Consequently, in the disk sample, $-\chi'$ is constant down to 4.2 K.

In Fig. 11, we give $-\chi'$ versus T for powdered sample, where $\text{GdBa}_2\text{Cu}_3\text{O}_{7-x}$ was mixed

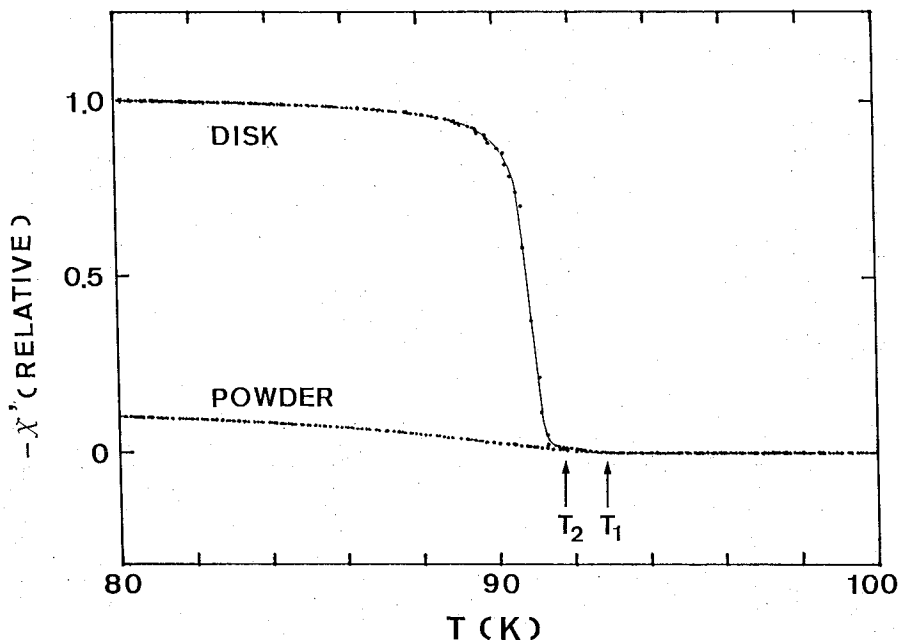


Fig. 9. Real components of the susceptibility for the disk and powdered $\text{GdBa}_2\text{Cu}_3\text{O}_{7-x}$ vs temperature, where $h_0=10$ mOe and $f=132$ Hz.

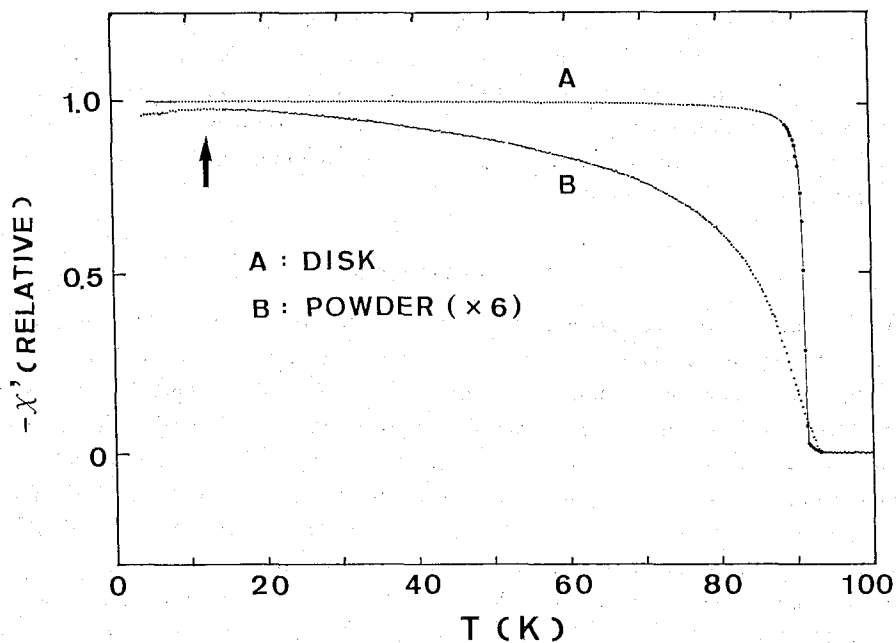


Fig. 10. Real components of the susceptibility for the disk and powdered $\text{GdBa}_2\text{Cu}_3\text{O}_{7-x}$ vs temperature, where $h_0=10$ mOe and $f=132$ Hz. The powdered sample has the maximum value at the temperature indicated by an arrow.

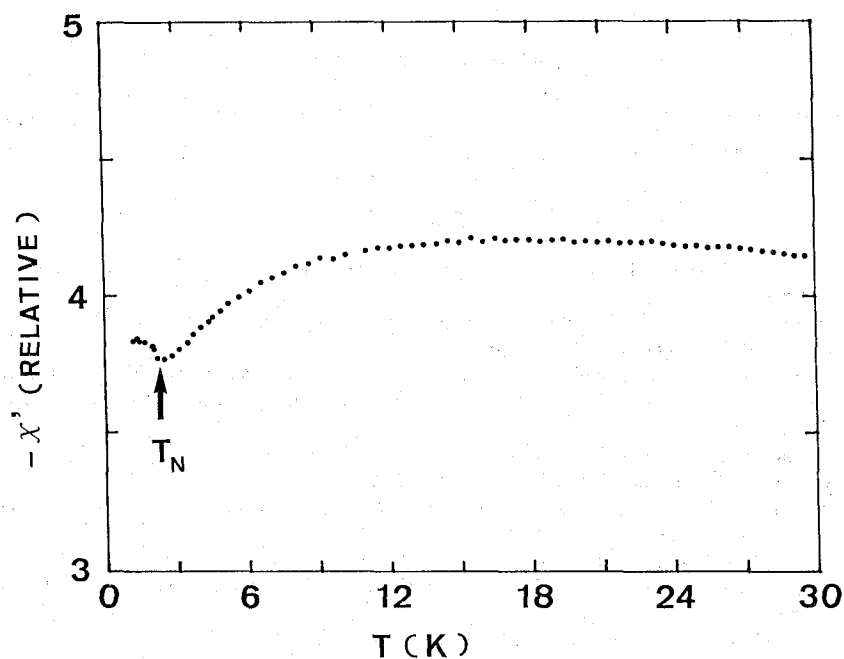


Fig. 11. Real component of the susceptibility for the powdered $\text{GdBa}_2\text{Cu}_3\text{O}_{7-x}$ vs temperature, where $h_0=1000$ mOe and $f=132$ Hz. T_N is the Neel temperature.

with the Al_2O_3 powder (1:2 in weight) and pressed. As seen there, $-\chi'$ has the minimum point at about 2.3 K. Since the reproducibility of this turning is excellent, it surely corresponds to the antiferromagnetic transition of Gd^{3+} ions. This result means the coexistence of the superconducting and the magnetic phases in the Gd-Ba-Cu-O system. Understanding of the mutual interaction between them would provide a key for the fundamental mechanism of the oxide superconductors.

IV. CONCLUSIONS

We measured the complex susceptibility and ac-resistive transition of $(\text{Y,Gd})\text{Ba}_2\text{Cu}_3\text{O}_{7-x}$ samples. The plausible conclusion is that in the temperature region just below the onset of χ' , fairly solid superconducting inclusions are produced. When the temperature is lowered further, these inclusions begin to couple and form a weak-link multiconnected network, where both χ' and χ'' become very sensitive to the amplitude h_0 of the external ac field. The transition width is broadened as h_0 increases. However, the onset temperature of χ' and χ'' stay constant for all h_0 measured. It has been also revealed that both χ' and χ'' are insensitive to the frequency of ac field below 320 Hz. These fundamental behaviors can be qualitatively understood by the phenomenological weak-link loop model. The smallness of the critical current density of oxide superconductors produced by the sintering treatment may come from this weak-link nature.

With the powdered sample of $\text{GdBa}_2\text{Cu}_3\text{O}_{7-x}$, we found the effect of paramagnetism of Gd^{3+} ions on χ' . The antiferromagnetic transition of the ions was also found in the curve of χ' at about 2.3 K.

ACKNOWLEDGMENT

The authors express their thanks to Dr. T. Ishida for preparation of one of the powdered $\text{GdBa}_2\text{Cu}_3\text{O}_{7-x}$ samples.

REFERENCES

- (1) R. Kanno, Y. Takeda, M. Hasegawa, O. Yamamoto, M. Takano, Y. Ikeda, and Y. Bando, *Mat. Res. Bull.*, **22** (1987) in press.
- (2) Y. Syono, M. Kikuchi, K. Ohishi, K. Hiraga, H. Arai, Y. Matsui, N. Kobayashi, T. Sasaoka, and Y. Muto, *Jpn. J. Appl. Phys.*, **26**, L498 (1987).
- (3) G. Van Tendeloo, H. W. Zandbergen, and S. Amelinckx, *Solid State Commun.* **63**, 389 (1987).
- (4) Y. Hirotsu, Y. Nakamura, Y. Murata, S. Nagakura, T. Nishihara, and M. Takata, *Jpn. J. Appl. Phys.*, **26**, L1168 (1987).
- (5) T. Ishida and H. Mazaki, *Phys. Rev. B*, **20**, 131 (1979).
- (6) T. Ishida and H. Mazaki, *J. Appl. Phys.*, **52**, 6798 (1981).
- (7) H. Mazaki, M. Takano, Z. Hiroi, Y. Bando, R. Kanno, Y. Takeda, and O. Yamamoto, *Bull. Inst. Chem. Res., Kyoto Univ.*, **65**, 147 (1987).
- (8) H. Mazaki, M. Takano, R. Kanno, and Y. Takeda, *Jpn. J. Appl. Phys.*, **6**, L780 (1987).
- (9) T. Takabatake, M. Ishikawa, Y. Nakazawa, I. Oguro, T. Sakakibara, and T. Goto, *Jpn. J. Appl. Phys.*, **26**, L978 (1987).
- (10) E. Maxwell and M. Strongin, *Phys. Rev. Lett.*, **10**, 212 (1963).
- (11) J. R. Thompson, S. T. Sekula, D. K. Christen, B. C. Sales, L. A. Boatner, and Y. C. Kim, *Phys. Rev. B*, **36**, 718 (1987).
- (12) T. Takabatake, Y. Nakazawa, and M. Ishikawa, *Jpn. J. Appl. Phys.*, **26**, L1231 (1987).